Journal of Zhejiang University-SCIENCE A (Applied Physics & Engineering)
ISSN 1673-565X (Print); ISSN 1862-1775 (Online)
www.jzus.zju.edu.cn; link.springer.com
E-mail: jzus_a@zju.edu.cn

Elemental mercury removal from coal gas by CeMnTi sorbents and their regeneration performance*

Hui CAO, Jin-song ZHOU†‡, Qi-xin ZHOU, Xin-yu XU, Cong XIE

State Key Laboratory of Clean Energy Utilization, Zhejiang University, Hangzhou 310027, China

†E-mail: zhoujs@zju.edu.cn

Received Feb. 29, 2020; Revision accepted Aug. 21, 2020; Crosschecked Feb. 24, 2021

Abstract: Ce and Mn modified TiO_2 sorbents (CeMnTi) were prepared by a co-precipitation method, and their ability to remove elemental mercury from coal gas in a fixed bed reactor was studied. Based on results of Brunauer-Emmett-Teller (BET), X-ray diffraction (XRD), scanning electron microscope (SEM), and X-ray photoelectron spectroscopy (XPS) studies, the modification mechanisms of the CeMnTi sorbents are discussed. Mn doping improved the specific surface area and dispersion of cerium oxides on the sorbent surface, while Ce doping increased the proportion of Mn^{4+} in manganese oxides by a synergetic effect between manganese oxides and cerium oxides. The effects of the active component, temperature, and coal gas components on the mercury removal performance of the sorbents were investigated. The results showed that the CeMnTi sorbents exhibited high mercury removal efficiency. $Ce_{0.2}Mn_{0.1}Ti$ adsorbed 91.55% elemental mercury from coal gas at 160 °C. H_2S and O_2 significantly improved the ability of sorbents to remove mercury. Part of the H_2S formed stable sulfates or sulfites through a series of oxidation reaction chains on the sorbent surface. HCl also improved the mercury removal performance, but reduced the promotion effect of H_2S for mercury removal when coexisting with H_2S. CO and H_2 had a minor inhibitory effect on mercury adsorption. The recycling performance of the sorbents was investigated by thermal regeneration. The thermal decomposition of the used sorbents indicated that mercury compounds were present mainly in the form of HgO and HgS, and higher temperature was beneficial for regeneration. The formation of sulfates and sulfites in the presence of H_2S led to a decrease in mercury removal efficiency.

Key words: CeMnTi; Synergistic effect; Gas components; Mercury removal; Thermal regeneration
https://doi.org/10.1631/jzus.A2000079 **CLC number:** TK16; X701

1 Introduction

Mercury is a highly toxic and volatile heavy metal with stable chemical properties, and accumulates in organisms and food chains for long durations. These properties have led to it being listed as a high priority for pollutant control. The main source of mercury pollution in the air is the combustion of fossil fuels, especially coal, natural gas and oil. According to International Energy Agency (IEA) projections (IEA, 2019), fossil fuels will continue to dominate global energy consumption in the next decade. Therefore, the harmful effects of mercury on humans and the environment will receive increasing attention by countries around the world.

As a promising clean coal utilization technology, coal gasification is characterized by high efficiency and cleanliness. It forms the basis of coal-based chemical synthesis, liquid fuel synthesis, oxygen production, poly generation systems, and other important process industries (Wang et al., 2009). Coal gasification transforms macromolecular coal into micromolecular combustible gases such as CO, H_2, and CH_4, which have a higher calorific value and cleaner combustion process than coal combustion. However, during the coal gasification process, the

‡ Corresponding author
* Project supported by the National Natural Science Foundation of China (No. 51576173)
ORCID: Hui CAO, https://orcid.org/0000-0002-4253-150X; Jin-song ZHOU, https://orcid.org/0000-0003-2704-0419

mercury contained in the coal is inevitably released into the coal gas. According to the literature (Lu et al., 2004), the mercury content in coal gas is much higher than that in flue gas. Moreover, the mercury in coal gas exists mainly in the form of elemental mercury, which is more difficult to remove than other forms of mercury. Currently, oxidation of Hg^0 to Hg^{2+} is the most common and effective method for chemical removal. Nevertheless, it is more difficult to remove elemental mercury from coal gas than from flue gas owing to its reducing behavior with CO, H_2, H_2S, and other reducing gases. A number of studies have focused mainly on the emission and control of mercury in coal-fired flue gas. Industrial applications involving injection of activated carbon for flue gas purification are common, but almost all of the sorbents have a very low physical adsorption performance for Hg^0. Therefore, research is focusing increasingly on the development of modified methods such as chemical adsorption to improve the performance of adsorbents for Hg^0 in flue gas (Liu and Adewuyi, 2016). For example, SO_2, NO, NO_2, the chlorine-based radicals in flue gas, and ozone strongly promote Hg^0 removal. Therefore, the use of these gases or the injection of corresponding substances can achieve efficient mercury removal or coordinated removal (Yuan et al., 2020). However, less attention has been paid to mercury removal from coal gas. Thus, with the rapid development of coal gasification technology, it is particularly important to strengthen basic research on mercury pollution control in the process of coal gasification, and to explore the mechanisms of mercury removal by sorbents in coal gas.

Sorbents with manganese oxides as their active component have been proved to exhibit an optimal mercury removal performance. Thus, the excellent catalytic performance of manganese oxides has been widely used for mercury removal from flue gas (Ji et al., 2008; Li et al., 2010; Yu et al., 2015). CeO_2 has been also widely studied and applied in the field of catalysis due to its strong oxygen storage capacity and superior catalytic performance (Reddy et al., 2003; Zhou et al., 2013). It has been observed to form Ce^{4+}/Ce^{3+} redox couples in the redox process, which have a good ability to store oxygen in oxygen deficient atmospheres and to release oxygen in oxygen excess atmospheres (Matsumoto, 2004). The combination of CeO_2 with other oxides such as manganese oxides may affect the surface structure of sorbents and the conversion of surface oxygen, thereby contributing to the adsorption and oxidation of mercury (Zhuang et al., 2012; Zhang HW et al., 2016; Li et al., 2018; Zhang SB et al., 2018). However, there has been no systematic study of the mechanism of mercury removal from coal gas by manganese cerium composite metal oxide sorbents.

Therefore, using TiO_2 with a defined pore structure and high specific surface area as carrier, sorbents have been modified by doping with Ce and Mn to enhance their adsorption capacity for mercury. In this study, a series of composite CeMnTi sorbents with different manganese and cerium contents were prepared by a co-precipitation method. Brunauer-Emmett-Teller (BET), X-ray diffraction (XRD), scanning electron microscope (SEM), X-ray photoelectron spectroscopy (XPS), and temperature-programmed reduction (TPR) were applied to characterize the structures and physicochemical properties of the sorbents, and the modification mechanisms were investigated. The efficiency of mercury removal from coal gas and the thermal regeneration performance of the sorbents were studied. The mechanisms of Hg^0 adsorption at different temperatures and in different coal gas atmospheres were also analyzed.

2 Experimental

2.1 Preparation of sorbents

The composite metal oxide sorbents were labeled Ce_xMn_yTi, where Ce represents CeO_2 and Ce_2O_3, Mn represents MnO_2 and Mn_2O_3, Ti represents TiO_2, x represents the CeO_2/TiO_2 mass ratio (x=0, 0.2, which refers to the optimal ratio of CeTi sorbents for mercury removal from coal gas according to our previous research (Zhou et al., 2013)), and y represents the MnO_2/TiO_2 mass ratio (y=0, 0.05, 0.1, 0.15, and 0.2). CeMnTi sorbents were prepared using a co-precipitation method. First, to attain different mass ratios, certain amounts of $Ce(NO_3)_3{\cdot}6H_2O$ (analytical reagent (AR)), $Mn(NO_3)_2{\cdot}6H_2O$ (AR), and nano-TiO_2 (Degussa P25, AR, Germany) were weighed and dissolved in deionized water by stirring. Subsequently, K_2CO_3 solution (0.1 g/mL) was added to adjust the pH to 8–9 under stirring, followed by precipitation and ageing. Next, the solution was suction filtered at

room temperature and washed to neutrality. Finally, the precipitate was collected and dried at 110 °C for 8 h. It was calcined at 500 °C for 2 h, followed by grinding and sieving to 60–80 meshes.

2.2 Mercury removal

The prepared sorbent was placed in a fixed-bed reactor (Fig. 1) for the adsorption experiments. As shown, the experimental system comprises mainly a simulated gas generation system, a mercury vapor generator, a fixed bed reactor, and an online mercury measurement system. About 50 mg of the sorbent was placed in a quartz tube reactor (10 mm in diameter) situated in a vertical tube furnace. The flow rate of the mercury vapor carrier N_2 and the temperature of the mercury vapor generator were adjusted such that the initial mercury concentration was stabilized at 55–60 μg/m^3. The total gas flow was maintained and controlled at 1.2 L/min by the mass flow controller (MFC), and the reaction time was 120 min. Adsorption temperatures of 30, 80, 120, 160, and 200 °C were used. The simulated atmosphere included N_2, H_2S, CO, H_2, and HCl. The mercury removal performance of the sorbents can be defined by the mercury removal efficiency η:

$$\eta=(Hg^0_{in}-Hg^0_{out})/Hg^0_{in}\times 100\%, \quad (1)$$

where Hg^0_{in} and Hg^0_{out} indicate the mercury concentration (μg/m^3) at the inlet and outlet of the quartz tube reactor, respectively.

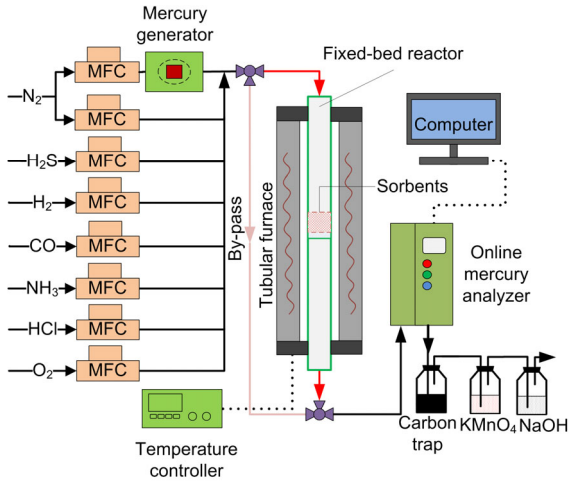

Fig. 1 Fixed-bed experimental device

2.3 Thermal desorption and regeneration

The thermal desorption and regeneration of the sorbents were also studied in the fixed-bed reactor. The specific process was as follows: the used sorbent was placed in the quartz tube reactor. The carrier gas was adjusted to be pure N_2, with the flow rate controlled to 1 L/min. The system was purged at room temperature for 30 min to remove the unstable mercury adsorbed on the sorbent surface, as well as the residual mercury vapor in the reactor. The carrier gas was adjusted again, and temperature programmed desorption regeneration was initiated.

2.4 Sorbent characterization

The characteristics of the sorbents and the modification mechanisms of Ce and Mn were studied by a series of characterization methods using fresh and used samples.

The specific surface area and pore parameters, which are key factors affecting the mercury removal performance of sorbents, were tested using an ASAP 2460 surface area and porosity analyzer (Micromeritics, the USA). The sorbent samples were degassed at 250 °C under vacuum for 4 h and subsequently subjected to N_2 adsorption at the liquid nitrogen temperature (196.15 °C). The specific surface area was calculated using the BET method, and the average pore diameter and total pore volume were calculated by the Barrett-Joyner-Halenda (BJH) method. XRD patterns were collected on a BRUKER D8 Advance X-ray diffractometer (Brook, Germany) to explore the atomic and molecular morphology of the sorbents. The target element and wavelength were Cu K-α (λ=0.154 nm), the tube voltage was 40 kV, and the tube current was 40 mA. The scanning range was 10°–80°, and the step size was 0.01°. SEM analysis was carried out using a Zeiss Sigma 500 microscope (Carl Zeiss, Germany) to gain insights about the surface morphology and structure of the samples. XPS was carried out using a Thermo Fisher Scientific K-α spectrometer (Thermo Fisher, the USA) to test the surface element valence and composition. The radiation source used in the XPS study was Al K-α ($h\nu$=1486.8 eV, where h is the Plank constant and ν is the frequency) with a power of 150 W. The transmission energy was fixed using the beam spot energy analyzer. The charge effect correction of the sample surface was calibrated by the C 1s standard

binding energy value of 284.8 eV, and curve fitting was performed using the peaking software XPS Peak 4.1. A TPR test was performed using a ChemBET Pulsar analyzer (Quantachrome, the USA). The gas was 10% CO/He (CO-TPR) and 10% H_2/He (H_2-TPR). The gas flow rate was 30 cm^3/min. The heating rate was 10 °C/min, and the heating range was 50–900 °C.

3 Results and discussion

3.1 Characterization

3.1.1 BET analysis

The BET surface area, average pore diameter, and total pore volume of the pure TiO_2 and CeMnTi sorbents are shown in Table 1. Most of the modified sorbents had larger specific surface areas and pore parameters than pure TiO_2, which meant that more active sites were available on the sorbents. The average pore diameter of nano-TiO_2 was 21.17 nm. The Ce and Mn improved the pore structure so that the pore sizes of the modified sorbents increased. The average pore diameters of all sorbents were in the range of mesopore, which facilitated the adsorption for macromolecular compounds such as HgO and HgS. In addition, the mesoporous structures could promote the mass transfer process in the catalytic oxidation reaction (Yu et al., 2015). Although micropores have a significant influence on the adsorption of mercury (the particle size of Hg is 2.6 μm), the physical adsorption of mercury molecules by micropores may not be as good as chemical binding by mesopores at high temperature.

Note that the pore parameters of $Ce_{0.2}Ti$ and $Ce_{0.2}Mn_{0.05}Ti$ were improved while their specific surface areas decreased due to sintering and agglomeration of partial metal oxides. Compared with the CeTi sorbent, the BET results of CeMnTi sorbents showed a slight improvement, which can be attributed to an increase in the dispersion of cerium oxides on the sorbent surface due to Mn doping. Also, the pore diameter decreased as the mass ratio of Mn exceeded 0.1, which might be related to the partial blockage of micropores due to excessive metal oxide loading (Shen et al., 2012). The BET surface area, average pore diameter, and total pore volume of $Ce_{0.2}Mn_{0.1}Ti$ reached 58.45 m^2/g, 31.08 nm, and 0.4792 cm^3/g, respectively. Overall, its textural properties were observed to be the best among the developed sorbents.

Table 1 BET surface area and pore parameters of sorbents

Sorbent	BET surface area (m^2/g)	Average pore diameter (nm)	Total pore volume (cm^3/g)
TiO_2	52.28	21.17	0.2691
$Ce_{0.2}Ti$	50.23	26.15	0.2835
$Ce_{0.2}Mn_{0.05}Ti$	52.25	28.44	0.3084
$Ce_{0.2}Mn_{0.1}Ti$	58.45	31.08	0.4792
$Ce_{0.2}Mn_{0.15}Ti$	58.93	23.90	0.3133
$Ce_{0.2}Mn_{0.2}Ti$	55.03	24.85	0.3148
$Mn_{0.2}Ti$	62.80	29.38	0.4594

3.1.2 XRD analysis

The XRD diffractograms are presented in Fig. 2. The XRD patterns of the sorbents were similar due to the obvious TiO_2 characteristic diffraction peaks, present mainly in the anatase form in all sorbents. Weak CeO_2 characteristic peaks (2θ=28.5°, 33.1°, 47.5°, 56.6°, and 59.19°) in CeTi sorbent could be observed. The characteristic peaks of MnO_2 (2θ= 28.6°, 37.3°, 42.7°, and 56.8°) were not significant in MnTi or CeMnTi sorbents, which may be due to the lower crystallinity of the manganese oxides on the sorbent surface (Wu et al., 2019). In addition, the intensity of the characteristic peak of CeO_2 decreased after loading Mn among CeTi and CeMnTi sorbents. This can be explained by monolayer dispersion theory (Mullins et al., 1998), which indicates that the active components have a high degree of dispersion on the surface of TiO_2. The metal oxides on the sorbent surface interact during the doping process to produce more amorphous metal oxides, which have higher activity than the crystalline metal oxides (Qi and Yang, 2004; Gao et al., 2010).

3.1.3 SEM analysis

SEM micrographs of the sorbents are shown in Fig. 3. The particles of the $Ce_{0.2}Ti$ and $Ce_{0.2}Mn_{0.05}Ti$ sorbents with a higher content of cerium oxides were uneven, and a fraction of oxides on the surface exhibited agglomeration and sintering. Also, Fig. 3a shows crystalline particles that were identified as metal oxides on the sorbent surface. In contrast, the $Mn_{0.2}Ti$ sorbent loaded with manganese oxides had a uniform surface and effective dispersion. The surface conditions of the sorbents carrying both cerium and

manganese oxides were intermediate. On increasing the manganese content, the surface structure of the sorbents showed a tendency for densification, followed by loosening, indicating that the addition of manganese can increase the dispersion of CeO_2 on the TiO_2 support. This was consistent with the findings from BET and XRD.

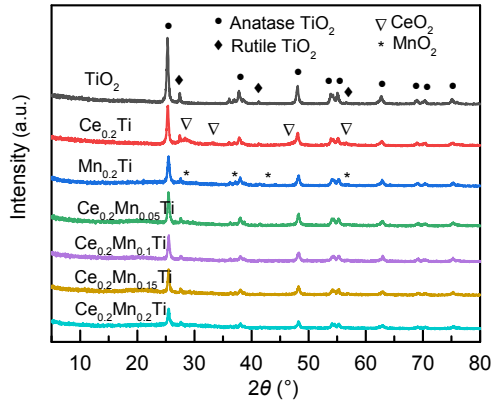

Fig. 2 XRD patterns of the sorbents

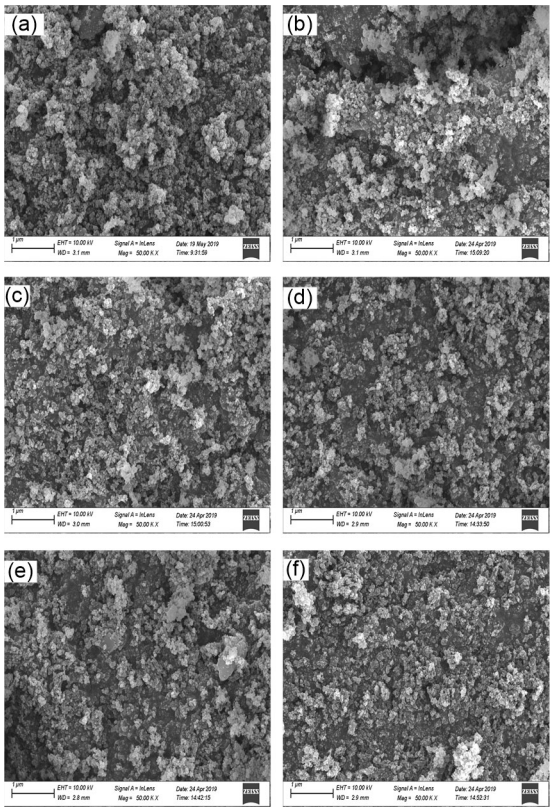

Fig. 3 SEM micrographs of the samples

(a) $Ce_{0.2}Ti$; (b) $Ce_{0.2}Mn_{0.05}Ti$; (c) $Ce_{0.2}Mn_{0.1}Ti$; (d) $Ce_{0.2}Mn_{0.15}Ti$; (e) $Ce_{0.2}Mn_{0.2}Ti$; (f) $Mn_{0.2}Ti$

3.1.4 XPS analysis

The XPS spectra of Ce 3d, Mn 2p, and O 1s are shown in Fig. 4. The atomic ratios of Ce, Mn, and O on the sorbent surface were calculated (Table 2). Fig. 4a shows the XPS spectrum of Ce 3d. The spectrum can be classified into two types of peaks (Reddy and Khan, 2005): Ce $3d_{3/2}$ and Ce $3d_{5/2}$, denoted by u and v, respectively. Among these, the u_0/v_0, u_2/v_2, u_3/v_3 pairs of peaks represent Ce^{4+}, and u_1/v_1 indicates Ce^{3+}. Two forms of Ce^{4+} and Ce^{3+} existed in the valence state of Ce on the sorbent surface. During the chemisorption process, the Ce^{4+}/Ce^{3+} electron pairs could participate in mercury removal by producing oxygen vacancies. Hence, the $Ce^{4+}/(Ce^{4+}+Ce^{3+})$ ratio was calculated to quantify the change in the Ce^{4+}/Ce^{3+} electron pairs. The $Ce^{4+}/(Ce^{4+}+Ce^{3+})$ ratios for fresh $Ce_{0.2}Ti$ and $Ce_{0.2}Mn_{0.1}Ti$ sorbents were 0.8634 and 0.8598, respectively (Table 2), which indicated that CeO_2 was the main cerium oxide, and the effect of the introduction of manganese on the Ce^{4+}/Ce^{3+} electron pairs was not obvious. After mercury adsorption, the $Ce^{4+}/(Ce^{4+}+Ce^{3+})$ ratio decreased to 0.6355, demonstrating that part of the CeO_2 was transformed to Ce_2O_3 during the mercury oxidation process.

Fig. 4b shows the Mn 2p XPS spectrum of the CeMnTi sorbent. The spectrum was fitted to two peaks (Zeng et al., 2017): Mn^{4+} with a binding energy of 642.93 eV, and Mn^{3+} with a binding energy of 641.69 eV. No peak of Mn^{2+} could be observed; thus, MnO_2 and Mn_2O_3 were regarded as the main manganese oxides on the sorbent surface. As higher valence manganese ions have a stronger ability to oxidize elemental mercury (Jampaiah et al., 2016), the $Mn^{4+}/(Mn^{4+}+Mn^{3+})$ ratio is important for mercury removal efficiency. The $Mn^{4+}/(Mn^{4+}+Mn^{3+})$ ratio was 0.3944 for fresh $Mn_{0.2}Ti$, and 0.4564 for the fresh $Ce_{0.2}Mn_{0.1}Ti$ sorbent, indicating that the addition of Ce increased the proportion of Mn^{4+} on the sorbent surface, thereby improving the oxidation performance of manganese. The $Mn^{4+}/(Mn^{4+}+Mn^{3+})$ ratio for $Ce_{0.2}Mn_{0.1}Ti$ changed from 0.4564 to 0.3291 during the mercury adsorption process, which may be attributed to the reduction of MnO_2 to Mn_2O_3 for oxidizing mercury. Ding et al. (1998) proposed a synergistic mechanism by the reaction chain between CeO_2 and MnO_2, which can be written as

$$Mn_2O_3 + 2CeO_2 \rightarrow 2MnO_2 + Ce_2O_3, \quad (2)$$

$$2MnO_2 \rightarrow Mn_2O_3 + [O], \quad (3)$$

where "[O]" represents the active oxygen.

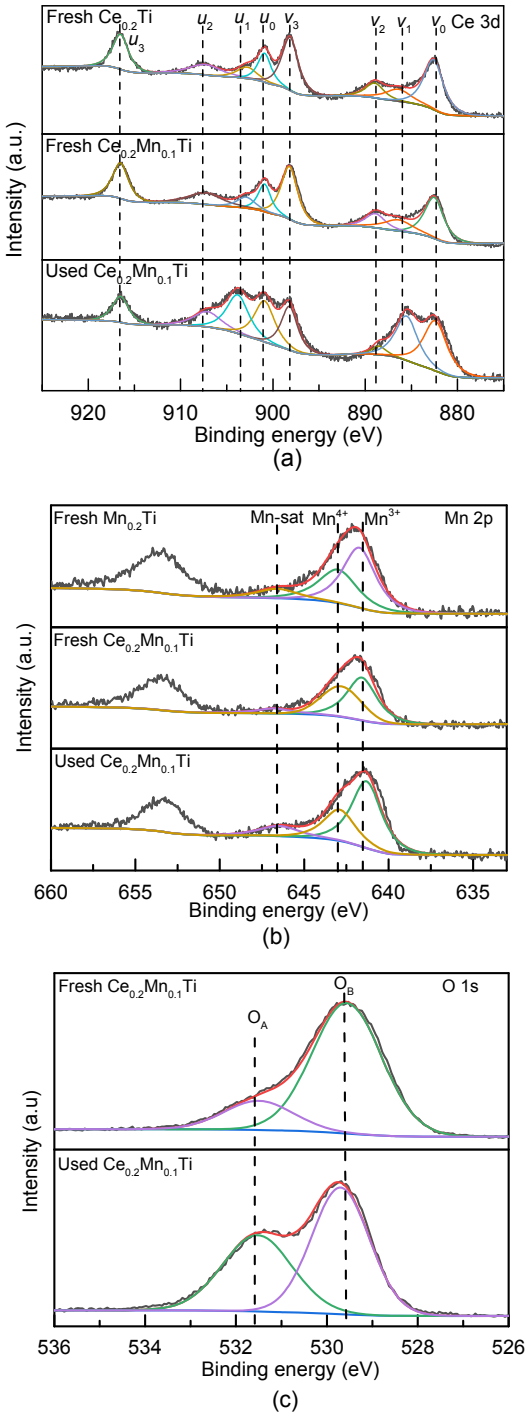

Fig. 4 Ce 3d XPS spectrum (a), Mn 2p XPS spectrum (b), and O 1s XPS spectrum (c) of the CeMnTi sorbents

Fig. 4c shows the O 1s XPS spectrum of $Ce_{0.2}Mn_{0.1}Ti$ sorbent. The O 1s peaks can be split into two peaks: O_A with a binding energy range of 531.3–531.9 eV, represents the chemisorbed oxygen, while O_B with a binding energy range of 529.3–530.0 eV, represents the lattice oxygen (Zhang et al., 2014). The $O_A/(O_A+O_B)$ ratio was 0.1810 before adsorption, and 0.4203 after adsorption. Compared with the fresh sorbent, the lattice oxygen of the $Ce_{0.2}Mn_{0.1}Ti$ sorbent was consumed significantly in the reaction process.

Table 2 Atomic ratios of Ce, Mn, and O to the total concentration of sorbents

Sorbent	$Ce^{4+}/(Ce^{4+}+Ce^{3+})$	$Mn^{4+}/(Mn^{4+}+Mn^{3+})$	$O_A/(O_A+O_B)$
Fresh $Ce_{0.2}Ti$	0.8634	–	0.2569
Fresh $Mn_{0.1}Ti$	–	0.3068	0.2306
Fresh $Mn_{0.2}Ti$	–	0.3944	0.2189
Fresh $Ce_{0.2}Mn_{0.1}Ti$	0.8598	0.4564	0.1810
Used $Ce_{0.2}Mn_{0.1}Ti$	0.6355	0.3291	0.4203

3.2 Effect of temperature

Adsorption temperature plays an important role in the removal of mercury from coal gas. The mercury removal efficiency of the sorbents increased initially, then decreased with increasing temperature in the experimental range (30–200 °C) (Fig. 5). This indicates that the sorbents exhibited two adsorption pathways, physical adsorption and chemisorption, to remove mercury from the coal gas. When the temperature was low, physical adsorption was dominant and the adsorption efficiency was positively related to the specific surface area. At higher temperatures, the physical adsorption weakened, and chemical adsorption became dominant due to the higher probability of molecular activity and collision. However, when the temperature exceeded 160 °C, the decomposition of HgO and HgS and the sublimation of active sulfur would be increased (You et al., 2014), leading to a decrease in mercury removal efficiency. Nevertheless, more than 83% Hg^0 removal efficiency could be obtained over $Ce_{0.2}Mn_{0.1}Ti$ at 200 °C. The adsorption efficiency of the CeMnTi sorbent in the temperature range of 80–160 °C remained stable. In particular, $Ce_{0.2}Mn_{0.1}Ti$ achieved the optimal physical and chemical adsorption performance, reaching an η value of 91.55% at 160 °C.

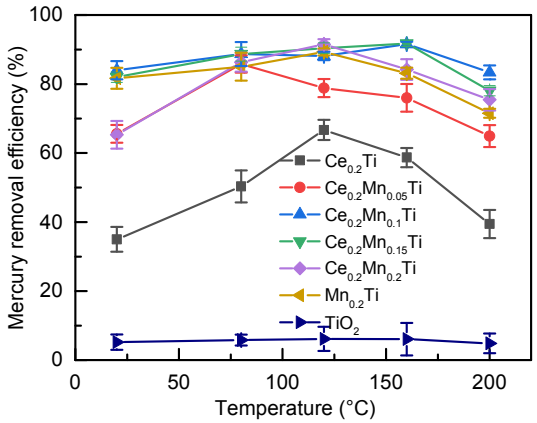

Fig. 5 Effect of temperature and active components on the mercury removal efficiency of the sorbents

3.3 Effect of active components

The adsorption performance of TiO_2 as support was not effective, while the mercury removal efficiency of $Ce_{0.2}Ti$ significantly increased (Fig. 5). Compared with the single cerium loading sorbent $Ce_{0.2}Ti$, the mercury removal efficiency of the composite metal oxide sorbents CeMnTi was also significantly improved. The $Ce_{0.2}Ti$ sorbent was noted to be less efficient than other sorbents owing to sintering agglomeration on the sorbent surface to form CeO_2 crystals, observed from the SEM and XRD patterns, which reduced the activity of the sorbent. On doping with Mn, the adsorption efficiency of the sorbents increased. However, when the Mn content was too high, the efficiency decreased to a certain extent, which may be related to the specific surface area of the sorbents and the dispersion of the active components. The mercury removal efficiency was consistent with the trend in the BET and SEM results, so it was inferred that the difference may be caused by the physical adsorption capacity of sorbents. Also, the $Ce_{0.2}Mn_{0.1}Ti$ and $Ce_{0.2}Mn_{0.15}Ti$ sorbents exhibited a higher mercury removal efficiency than $Ce_{0.2}Ti$ and $Mn_{0.2}Ti$, which was attributed to the interaction between Ce and Mn (Eqs. (2) and (3)).

For the CeMnTi sorbents, the values of η were stable, and $Ce_{0.2}Mn_{0.1}Ti$ and $Ce_{0.2}Mn_{0.15}Ti$ reached more than 85% in the temperature range of 80–160 °C. Based on the observed results, the $Ce_{0.2}Mn_{0.1}Ti$ sorbent and an adsorption temperature of 160 °C were selected for further experiments.

3.4 Effect of coal gas components

3.4.1 Effect of H_2S

The mercury removal efficiency of the $Ce_{0.2}Mn_{0.1}Ti$ sorbent under pure N_2 conditions was 46.29% (Fig. 6). On introducing 80 ppm (1 ppm=1×10^{-6}) H_2S, the mercury removal performance was obviously improved to 65.47%. On continuously increasing the concentration of H_2S to 400 ppm, the mercury removal efficiency rose to 91.55%. Obviously, the presence of H_2S contributed to the removal of Hg^0. The oxidation process of Hg^0 on the sorbent surface follows the Mars-Maessen mechanism (Granite et al., 2000), i.e. the gas phase Hg^0 is first adsorbed on the sorbent surface, followed by oxidization with the active oxygen in the sorbent to form HgO:

$$Hg^0_{(g)} + \text{surface} \rightarrow Hg^0_{(ad)}, \quad (4)$$

$$Hg^0_{(ad)} + [O] \rightarrow HgO, \quad (5)$$

where "(ad)" represents the adsorbed state.

As a reducing gas, H_2S was not able to oxidize Hg^0 by itself. In the presence of the $Ce_{0.2}Mn_{0.1}Ti$ sorbent, the oxygen in the sorbent reacted with H_2S to promote further oxidation of Hg^0. As mentioned earlier, the presence of the Ce^{4+}/Ce^{3+} electron pair provides a large number of oxygen vacancies and reactive oxygen for the H_2S promotion process, which is:

$$H_2S+[O] \rightarrow S_{(ad)}+H_2O, \quad (6)$$

$$S_{(ad)}+Hg^0_{(ad)} \rightarrow HgS. \quad (7)$$

A small amount of light yellow matter was found at the end of the quartz tube reactor on introducing 400 ppm H_2S. The melting point of elemental sulfur is about 126 °C and the decomposition temperature of HgS was relatively high (Lu et al., 2012). Therefore, this might be attributed to the condensation of partially sublimated active sulfur (Eq. (6)), which suggests that 400 ppm H_2S was excessive for mercury removal. To verify the morphology of elemental sulfur species after mercury and H_2S adsorption, XPS was applied to characterize the used samples. The peaks at 162.44 eV and 163.68 eV (Fig. 7) were attributed to S^{2-} and S, respectively (Yang et al., 2018),

which proved the generation of active sulfur and HgS (Eqs. (6) and (7)). In addition, the peaks at 167.14 eV and 168.71 eV were assigned to sulfite and sulfate, respectively (Andreu et al., 2015), indicating the formation of metal sulfites and sulfates. The metal sulfites and sulfates, such as manganese sulfates and cerium sulfates, are stable during regeneration (Cheah et al., 2009), resulting in a loss of active material. Therefore, future studies could further explore the chemical reaction chains and morphology of elemental sulfur over the CeMnTi sorbents to avoid the formation of sulfites and sulfates.

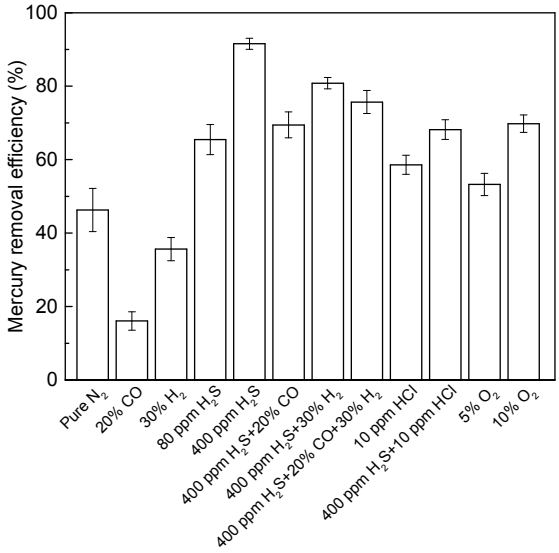

Fig. 6 Effect of coal gas components on the mercury removal efficiency of $Ce_{0.2}Mn_{0.1}Ti$ at 160 °C

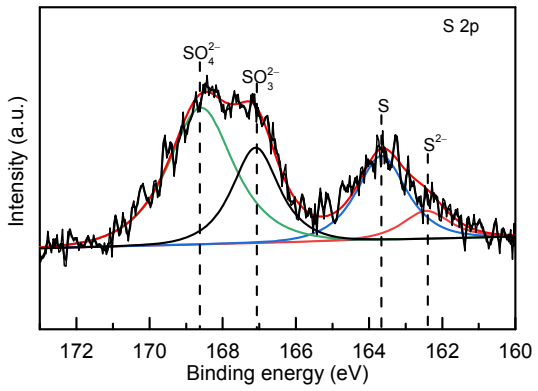

Fig. 7 S 2p XPS spectrum of the used $Ce_{0.2}Mn_{0.1}Ti$ sorbent

3.4.2 Effect of CO and H_2

CO and H_2 are the main components in coal gas. Thus, it is also necessary to study the effect of CO and H_2 on mercury removal by CeMnTi sorbents. Specifically, the effect of CO and H_2 on the mercury removal of the sorbents was investigated under pure N_2 and N_2+H_2S conditions. On introducing 20% CO or 30% H_2 into pure N_2, the values of η decreased from 46.29% to 16.08% and 34.51%, respectively. As strong reducing agents, CO and H_2 can reduce active components on the sorbent surface. However, as shown in Fig. 8, there was no significant difference between CO and H_2 when the temperature was in the range of 0–200 °C. Therefore, the reason for the stronger inhibition by CO might be its stronger competitiveness for the active adsorption sites.

On introducing H_2S, CO and H_2 had no obvious influence on Hg^0 capture, which demonstrated that H_2S played a key role in mercury removal from the coal gas. In the presence of H_2S and CO, the value of η was lower than that in N_2 with H_2S. This was because CO reacted with H_2S and active sulfur to form COS (Eq. (8)), which seized the active adsorption sites, thereby, inhibiting the adsorption of mercury (Wu et al., 2007). For H_2, it was easily adsorbed on the sorbent surface and protonated to H^+ (Zhang et al., 2012), which consumed the active oxygen and suppressed the generation of active sulfur. Furthermore, Kobayashi and Flytzani-Stephanopoulos (2002) proposed that H_2 could partially consume active sulfur by reacting with H_2S and CeO_2 (Eq. (9)), which was also not conductive to mercury removal.

Nevertheless, the coexistence of CO and H_2 promoted Hg^0 adsorption compared with CO. This may have been due to the increase in H_2 concentration, which hindered reaction Eq. (8), thereby reducing the consumption of active sulfur.

$$H_2S+CO \rightarrow COS+H_2, \quad (8)$$

$$2CeO_2S+H_2S+H_2 \rightarrow CeO_2S+2H_2O. \quad (9)$$

3.4.3 Effect of HCl

HCl is considered to be one of the most critical components affecting mercury oxidation in flue gas (Zheng et al., 2012). Therefore, the effect of HCl on the mercury removal of the CeMnTi sorbent in coal gas was also studied in this work. The mercury removal efficiency of the CeMnTi sorbent increased from 46.29% to 68.17% as 10 ppm HCl was introduced into pure N_2 (Fig. 6) indicating that HCl could

promote the removal of mercury. HCl could react with the active oxygen to form active chlorine, followed by further chemical reaction with the adsorbed mercury (Li et al., 2011). However, in the presence of H_2S, the introduction of HCl caused a decrease in mercury removal efficiency, which might have been due to competition between HCl and H_2S. HCl and H_2S may have competed with elemental mercury for the active adsorption sites, resulting in a reduced amount of mercury adsorbed on the surface (Hou et al., 2014). Alternatively, HCl may have consumed a part of the active oxygen to weaken the promotion of mercury removal by H_2S.

$$2HCl+[O] \rightarrow 2[Cl]+H_2O, \quad (10)$$

$$Hg_{(ad)}+[Cl] \rightarrow HgCl, \quad (11)$$

$$HgCl+[Cl] \rightarrow HgCl_2. \quad (12)$$

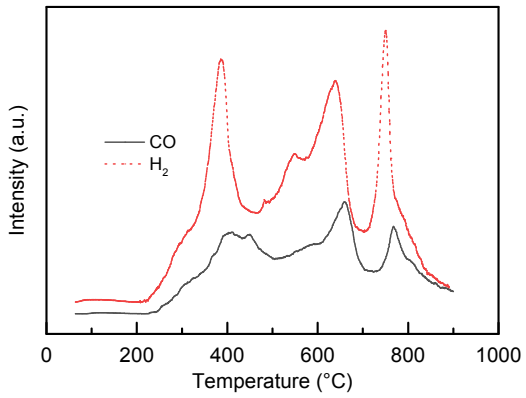

Fig. 8 TPR patterns of CO and H_2 for the $Ce_{0.2}Mn_{0.1}Ti$ sorbent

3.4.4 Effect of O_2

He et al. (2014) found that the gas phase O_2 in flue gas could supply the lattice oxygen consumed in the reaction process. Therefore, the effect of O_2 on mercury removal performance was tested. The introduction of oxygen facilitated the removal of mercury (Fig. 6). When 5% O_2 was introduced, the mercury removal efficiency of the sorbent increased to 53.25%. When the concentration of O_2 was raised to 10%, the mercury removal efficiency increased further to 69.80%. Thus, under aerobic conditions, the presence of oxygen was conducive to the adsorption and oxidation of mercury.

3.5 Thermal desorption and regeneration

The regeneration performance of the sorbent has an important influence on reducing the operational cost and environmental risks (Dong et al., 2009). Thus, the regeneration performance of the CeMnTi sorbent was investigated using the thermal desorption regeneration method.

To further explore the mercury desorption performance of the used $Ce_{0.2}Mn_{0.1}Ti$ sorbents (the sorbents adsorbed mercury at 160 °C, N_2+400 ppm H_2S for 2 h), a series of temperature-programmed desorption experiments were carried out. The mercury desorption curves of 500 °C+N_2, 500 °C+5% O_2+N_2, and 400 °C+5% O_2+N_2 using a heating rate of 10 °C/min were collected (Fig. 9). The desorption pathway of mercury was observed to be as follows: mercury started to release from the sorbents at 180–200 °C, which suggests that it was chemisorbed on the used $Ce_{0.2}Mn_{0.1}Ti$ surface. On increasing the heating temperature, the main desorption peak of mercury occurred at around 300 °C. In particular, the secondary peak was observed at about 500 °C. Note that during the desorption process, only a small amount of Hg^{2+} was detected at the beginning of the mercury desorption phase. In other words, mercury was largely desorbed in the form of elemental mercury, indicating that the mercury compounds bound to the sorbent surface were decomposed into elemental mercury, followed by removal with other gases by the carrier gas.

The decomposition temperatures of the pure mercury compounds (Rallo et al., 2014; Rumayor et al., 2015) are shown in Table 3. Note that due to the catalytic action of the carrier and active components, a certain deviation in the mercury desorption existed in the actual sorbents. Combining the previous analysis with the desorption curves of mercury, the desorption peak centered at about 300 °C corresponded to the decomposition of HgO (HgO yellow and HgO red) and HgS red, while that at about 500 °C might be attributed to the decomposition of HgO (HgO yellow and HgO red) and a small quantity of $HgSO_4$. Moreover, this also illustrates that the mercury existed mainly in the form of HgO and HgS on the sorbent surface.

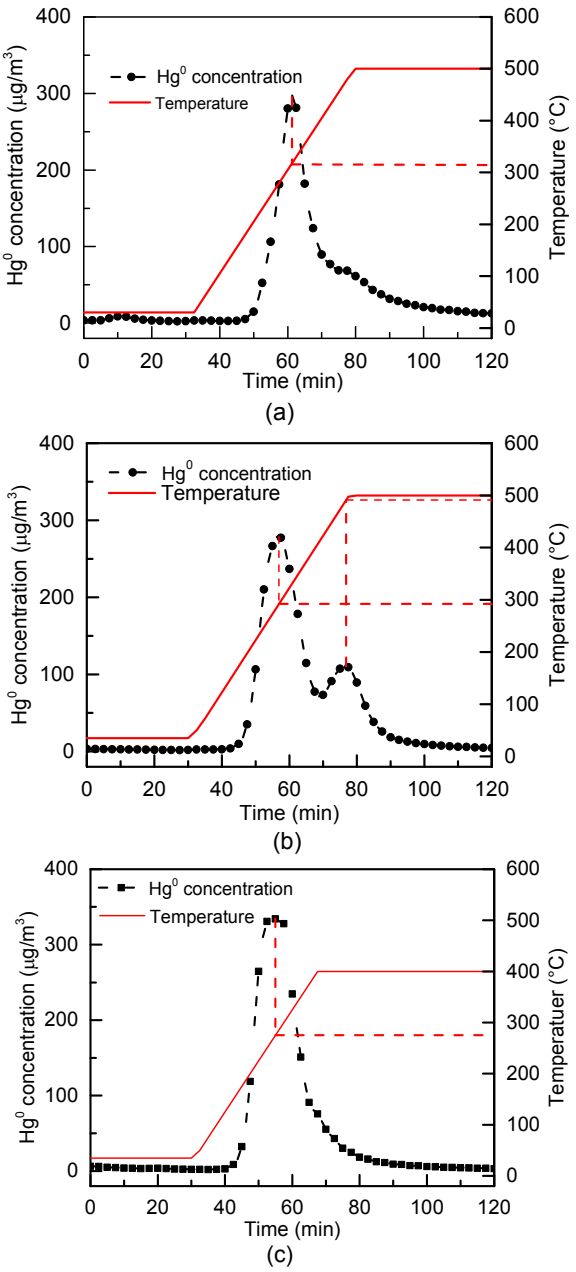

Fig. 9 Mercury desorption curves for the $Ce_{0.2}Mn_{0.1}Ti$ sorbent under different temperatures and atmospheric conditions. Reaction conditions: (a) 500 °C+N_2; (b) 500 °C+5% O_2+N_2; (c) 400 °C+5% O_2+N_2

After studying the mercury desorption, the mercury adsorption performance of the sorbents was re-tested (Fig. 10). The regeneration temperature had a more significant effect on the mercury removal efficiency of the CeMnTi sorbent than the introduction of 5% O_2. The mercury removal efficiency of the fresh $Ce_{0.2}Mn_{0.1}Ti$ sorbent was 91.55%, while it was reduced to 72.83% after regeneration at 500 °C under N_2 with 5% O_2. This shows that the higher regeneration temperature could desorb most of mercury compounds and restore the occupied active sites. After the introduction of 5% O_2, the mercury removal efficiency improved slightly (from 70.25% to 72.83%). This may have been due to the O_2 molecules oxidizing the low valence oxides on the sorbent surface, thereby supplementing the active oxygen required for the adsorption reaction. Zeng et al. (1999) conducted research with modified ceria. Their ceria regeneration scheme consisted of:

$$2Ce_2O_3+O_2 \rightarrow 4CeO_2, \quad (13)$$

$$Ce_2O_2S+O_2 \rightarrow 2CeO_2+S_{(g)}, \quad (14)$$

$$Mn_2O_3+2CeO_2 \rightarrow 2MnO_2+Ce_2O_3. \quad (15)$$

A synergistic effect of Mn and Ce existing in the modification (Eq. (15)) also worked during the regeneration process.

Regeneration under different oxygen concentrations was studied (Fig. 11). The oxygen concentration had a limited effect on regeneration efficiency when it exceeded 5%. O_2 can oxidize low-priced metal oxides to restore the partly adsorbed active sites (Zhu et al., 2018). However, Table 3 shows that the sorbent provided a large amount of active oxygen and consumed less active oxygen in mercury removal. Further, the regeneration (under 5% O_2) after the mercury removal reaction in pure N_2 (without H_2S) was studied. The decrease in mercury removal efficiency was reduced compared with mercury removal in H_2S (Fig. 12). Thus, we conclude that the smaller O_2 effect, as suggested earlier, may be due to the formation of some metal sulfates and sulfites, resulting in the loss of active components and hindering the decomposition of mercury compounds.

Table 3 Decomposition temperatures of the pure mercury compounds

Mercury compound	Decomposition peak temperature (°C)	Decomposition temperature range (°C)
HgO yellow	284±7; 469±6	190–380; 320–530
HgO red	308±1; 471±5	200–360; 370–530
HgS black	190±11	150–280
HgS red	260±10	250–400
$HgSO_4$	583±8	500–600

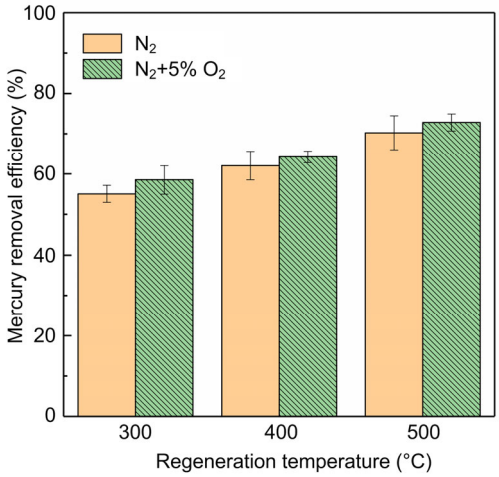

Fig. 10 Mercury removal efficiency after regeneration under different temperatures and atmospheric conditions. Mercury adsorption conditions: N_2 with 400 ppm H_2S, about 55 μg/m^3 Hg^0, 160 °C

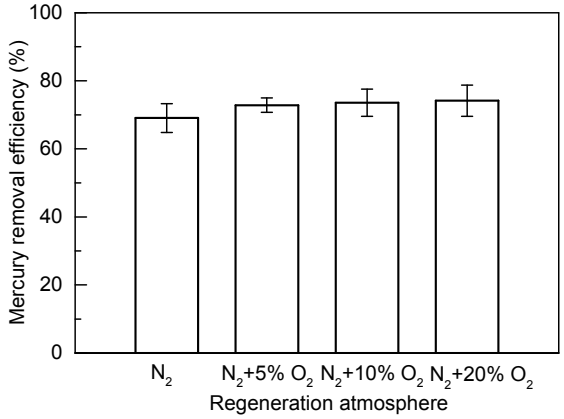

Fig. 11 Regeneration under different oxygen concentrations

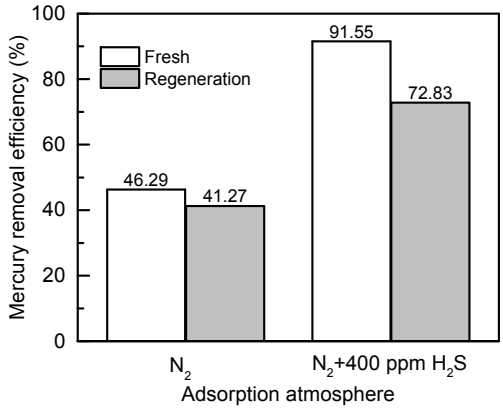

Fig. 12 Regeneration under different adsorption atmospheres

4 Conclusions

CeMnTi sorbents were prepared by a co-precipitation method, and their performance and mechanisms involved in removing mercury from coal gas were studied. Several meaningful observations were made in this study:

1. The $Ce_{0.2}Mn_{0.1}Ti$ sorbent displayed higher mercury removal efficiency and thermal stability than the CeTi and MnTi sorbents. Its mercury removal efficiency reached 91.55% at 160 °C and remained above 83% at 200 °C.

2. Mn doping improves the BET surface area and dispersion of cerium oxides on the sorbent surface, while Ce doping could increase the proportion of Mn^{4+} by the interaction with manganese oxides.

3. H_2S significantly promoted the adsorption of mercury by generating active sulfur on the sorbent surface. However, H_2S could react with active components to form sulfates and sulfites, making it difficult for sorbent regeneration. The presence of CO and H_2 inhibited mercury removal. HCl improved mercury removal performance, but had the opposite effect when combined with H_2S due to competition for mercury.

4. The mercury compounds on the sorbent existed mainly in the form of HgO and HgS, and most could be desorbed at 500 °C. The main reason for a decrease in mercury removal efficiency may be the formation of sulfates and sulfites in the presence of H_2S.

Contributors

Hui CAO wrote the manuscript. Jin-song ZHOU and Qi-xin ZHOU provided the suggestions. Qi-xin ZHOU, Xin-yu XU, and Cong XIE helped to organize the manuscript.

Conflict of interest

Hui CAO, Jin-song ZHOU, Qi-xin ZHOU, Xin-yu XU, and Cong XIE declare that they have no conflict of interest.

Reference

Andreu N, Flahaut D, Dedryvère R, et al., 2015. XPS investigation of surface reactivity of electrode materials: effect of the transition metal. *ACS Applied Materials & Interfaces*, 7(12):6629-6636. https://doi.org/10.1021/am5089764

Cheah S, Carpenter DL, Magrini-Bair KA, 2009. Review of mid- to high-temperature sulfur sorbents for desulfurization of biomass- and coal-derived syngas. *Energy & Fuels*,

23(11):5291-5307.
https://doi.org/10.1021/ef900714q

Ding ZY, Li LX, Wade D, et al., 1998. Supercritical water oxidation of NH_3 over a MnO_2/CeO_2 catalyst. *Industrial & Engineering Chemistry Research*, 37(5):1707-1716.
https://doi.org/10.1021/ie9709345

Dong J, Xu ZH, Kuznicki SM, 2009. Mercury removal from flue gases by novel regenerable magnetic nanocomposite sorbents. *Environmental Science & Technology*, 43(9): 3266-3271.
https://doi.org/10.1021/es803306n

Gao X, Jiang Y, Zhong Y, et al., 2010. The activity and characterization of CeO_2-TiO_2 catalysts prepared by the sol-gel method for selective catalytic reduction of NO with NH_3. *Journal of Hazardous Materials*, 174(1-3): 734-739.
https://doi.org/10.1016/j.jhazmat.2009.09.112

Granite EJ, Pennline HW, Hargis RA, 2000. Novel sorbents for mercury removal from flue gas. *Industrial & Engineering Chemistry Research*, 39(4):1020-1029.
https://doi.org/10.1021/ie990758v

He C, Shen BX, Chen JH, et al., 2014. Adsorption and oxidation of elemental mercury over Ce-MnO_x/Ti-PILCs. *Environmental Science & Technology*, 48(14):7891-7898.
https://doi.org/10.1021/es5007719

Hou WH, Zhou JS, Qi P, et al., 2014. Effect of H_2S/HCl on the removal of elemental mercury in syngas over CeO_2-TiO_2. *Chemical Engineering Journal*, 241:131-137.
https://doi.org/10.1016/j.cej.2013.12.047

IEA (International Energy Agency), 2019. World Energy Outlook 2019.
https://www.iea.org/reports/world-energy-outlook-2019

Jampaiah D, Ippolito SJ, Sabri YM, et al., 2016. Ceria-zirconia modified MnO_x catalysts for gaseous elemental mercury oxidation and adsorption. *Catalysis Science & Technology*, 6(6):1792-1803.
https://doi.org/10.1039/c5cy01534k

Ji L, Sreekanth PM, Smirniotis PG, et al., 2008. Manganese oxide/titania materials for removal of NO_x and elemental mercury from flue gas. *Energy & Fuels*, 22(4):2299-2306.
https://doi.org/10.1021/ef700533q

Kobayashi M, Flytzani-Stephanopoulos M, 2002. Reduction and sulfidation kinetics of cerium oxide and Cu-modified cerium oxide. *Industrial & Engineering Chemistry Research*, 41(13):3115-3123.
https://doi.org/10.1021/ie010815w

Li HL, Wu CY, Li Y, et al., 2011. CeO_2-TiO_2 catalysts for catalytic oxidation of elemental mercury in low-rank coal combustion flue gas. *Environmental Science & Technology*, 45(17):7394-7400.
https://doi.org/10.1021/es2007808

Li JF, Yan NQ, Qu Z, et al., 2010. Catalytic oxidation of elemental mercury over the modified catalyst Mn/α-Al_2O_3 at lower temperatures. *Environmental Science & Technology*, 44(1):426-431.
https://doi.org/10.1021/es9021206

Li XQ, Zhou JS, Zhou QX, et al., 2018. Removal of elemental mercury using titania sorbents loaded with cobalt ceria oxides from syngas. *New Journal of Chemistry*, 42(15): 12503-12510.
https://doi.org/10.1039/C8NJ02069H

Liu YX, Adewuyi YG, 2016. A review on removal of elemental mercury from flue gas using advanced oxidation process: chemistry and process. *Chemical Engineering Research and Design*, 112:199-250.
https://doi.org/10.1016/j.cherd.2016.06.024

Lu DY, Granatstein DL, Rose DJ, 2004. Study of mercury speciation from simulated coal gasification. *Industrial & Engineering Chemistry Research*, 43(17):5400-5404.
https://doi.org/10.1021/ie034121u

Lu H, Greenwood P, Chen TS, et al., 2012. The separate production of H_2S from the thermal reaction of hydrocarbons with magnesium sulfate and sulfur: implications for thermal sulfate reduction. *Applied Geochemistry*, 27(1): 96-105.
https://doi.org/10.1016/j.apgeochem.2011.09.007

Matsumoto S, 2004. Recent advances in automobile exhaust catalysts. *Catalysis Today*, 90(3-4):183-190.
https://doi.org/10.1016/j.cattod.2004.04.048

Mullins DR, Overbury SH, Huntley DR, 1998. Electron spectroscopy of single crystal and polycrystalline cerium oxide surfaces. *Surface Science*, 409(2):307-319.
https://doi.org/10.1016/S0039-6028(98)00257-X

Qi GS, Yang RT, 2004. Characterization and FTIR studies of MnO_x-CeO_2 catalyst for low-temperature selective catalytic reduction of NO with NH_3. *The Journal of Physical Chemistry B*, 108(40):15738-15747.
https://doi.org/10.1021/jp048431h

Rallo M, Fuente-Cuesta A, Lopez-Anton MA, et al., 2014. Speciation of Hg retained in gasification biomass chars by temperature-programmed decomposition. *Fuel Processing Technology*, 126:1-4.
https://doi.org/10.1016/j.fuproc.2014.04.010

Reddy BM, Khan A, 2005. Nanosized CeO_2-SiO_2, CeO_2-TiO_2, and CeO_2-ZrO_2 mixed oxides: influence of supporting oxide on thermal stability and oxygen storage properties of ceria. *Catalysis Surveys from Asia*, 9(3):155-171.
https://doi.org/10.1007/s10563-005-7552-1

Reddy BM, Khan A, Yamada Y, et al., 2003. Structural characterization of CeO_2-TiO_2 and V_2O_5/CeO_2-TiO_2 catalysts by Raman and XPS techniques. *The Journal of Physical Chemistry B*, 107(22):5162-5167.
https://doi.org/10.1021/jp0344601

Rumayor M, Fernandez-Miranda N, Lopez-Anton MA, et al., 2015. Application of mercury temperature programmed desorption (HgTPD) to ascertain mercury/char interactions. *Fuel Processing Technology*, 132:9-14.
https://doi.org/10.1016/j.fuproc.2014.12.032

Shen BX, Ma HQ, Yao Y, 2012. Mn-CeO_x/Ti-PILCs for selective catalytic reduction of NO with NH_3 at low temperature. *Journal of Environmental Sciences*, 24(3): 499-506.

https://doi.org/10.1016/S1001-0742(11)60756-0

Wang FC, Yu GS, Gong X, et al., 2009. Research and development of large-scale coal gasification technology. *Chemical Industry and Engineering Progress*, 28(2):173-180. https://doi.org/10.3321/j.issn:1000-6613.2009.02.001

Wu SJ, Oya N, Ozaki M, et al., 2007. Development of iron oxide sorbents for Hg^0 removal from coal derived fuel gas: sulfidation characteristics of iron oxide sorbents and activity for COS formation during Hg^0 removal. *Fuel*, 86(17-18):2857-2863. https://doi.org/10.1016/j.fuel.2007.03.004

Wu X, Duan YF, Yao T, et al., 2019. Mercury removal performance and SO_2 resistance of Ce-Mn/TiO_2 sorbent. *China Environmental Science*, 39(6):2336-2343. https://doi.org/10.19674/j.cnki.issn1000-6923.2019.0278

Yang ZQ, Li HL, Liao C, et al., 2018. Magnetic rattle-type Fe_3O_4@CuS nanoparticles as recyclable sorbents for mercury capture from coal combustion flue gas. *ACS Applied Nano Materials*, 1(9):4726-4736. https://doi.org/10.1021/acsanm.8b00948

You SL, Zhou JS, Hou WH, et al., 2014. Factors influencing the removal of elemental mercury by Mn-AC sorbent in syngas. *Journal of Fuel Chemistry and Technology*, 42(11):1324-1331. https://doi.org/10.3969/j.issn.0253-2409.2014.11.008

Yu XQ, Bao JJ, Jiang XX, et al., 2015. Performance and mechanism of catalytic oxidation for mercury by Mn-doped TiO_2 catalysts in flue gas. *Proceedings of the CSEE*, 35(13):3331-3337. https://doi.org/10.13334/j.0258-8013.pcsee.2015.13.016

Yuan B, Mao XZ, Wang Z, et al., 2020. Radical-induced oxidation removal of multi-air-pollutant: a critical review. *Journal of Hazardous Materials*, 383:121162. https://doi.org/10.1016/j.jhazmat.2019.121162

Zeng XB, Xu Y, Zhang B, et al., 2017. Elemental mercury adsorption and regeneration performance of sorbents $FeMnO_x$ enhanced via non-thermal plasma. *Chemical Engineering Journal*, 309:503-512. https://doi.org/10.1016/j.cej.2016.10.047

Zeng Y, Zhang S, Groves FR, et al., 1999. High temperature gas desulfurization with elemental sulfur production. *Chemical Engineering Science*, 54(15-16):3007-3017. https://doi.org/10.1016/S0009-2509(98)00427-8

Zhang AC, Zheng WW, Song J, et al., 2014. Cobalt manganese oxides modified titania catalysts for oxidation of elemental mercury at low flue gas temperature. *Chemical Engineering Journal*, 236:29-38. https://doi.org/10.1016/j.cej.2013.09.060

Zhang H, Zhao JT, Fang YT, et al., 2012. Catalytic oxidation and stabilized adsorption of elemental mercury from coal-derived fuel gas. *Energy & Fuels*, 26(3):1629-1637. https://doi.org/10.1021/ef201453d

Zhang HW, Chen JY, Zhao K, et al., 2016. Removal of vapor-phase elemental mercury from simulated syngas using semi-coke modified by Mn/Ce doping. *Journal of Fuel Chemistry and Technology*, 44(4):394-400. https://doi.org/10.1016/S1872-5813(16)30020-2

Zhang SB, Zhao YC, Díaz-Somoano M, et al., 2018. Synergistic mercury removal over the $CeMnO_3$ perovskite structure oxide as a selective catalytic reduction catalyst from coal combustion flue gas. *Energy & Fuels*, 32(11):11785-11795. https://doi.org/10.1021/acs.energyfuels.8b02518

Zheng JM, Zhou JS, Luo ZY, et al., 2012. Impact of individual acid flue gas components on mercury capture by heat-treated activated carbon. *Journal of Zhejiang University-SCIENCE A (Applied Physics & Engineering)*, 13(9):700-708. https://doi.org/10.1631/jzus.A1200112

Zhou JS, Hou WH, Qi P, et al., 2013. CeO_2-TiO_2 sorbents for the removal of elemental mercury from syngas. *Environmental Science & Technology*, 47(17):10056-10062. https://doi.org/10.1021/es401681y

Zhu YC, Han XJ, Huang ZG, et al., 2018. Superior activity of CeO_2 modified V_2O_5/AC catalyst for mercury removal at low temperature. *Chemical Engineering Journal*, 337:741-749. https://doi.org/10.1016/j.cej.2017.10.115

Zhuang K, Qiu J, Xu BL, et al., 2012. Promotional effect of cerium oxide on the catalytic properties of Ce-Mn-Ti-O catalysts for selective catalytic reduction of NO. *Acta Physico-Chimica Sinica*, 28(3):681-685. https://doi.org/10.3866/PKU.WHXB201111141